Temperature-dependent Raman scattering and x-ray diffraction study of phase transitions in layered multiferroic $CuCrP_2S_6$

M. A. Susner,[1,2] R. Rao,[1,2] A. T. Pelton,[1,2] M. V. McLeod,[3,4] and B. Maruyama[1]

[1]*Materials and Manufacturing Directorate, Air Force Research Laboratory, Wright-Patterson Air Force Base, Ohio 45433, USA*

[2]*UES, Inc., 4401 Dayton-Xenia Road, Dayton, Ohio 45432, USA*

[3]*Aerospace Systems Directorate, Air Force Research Laboratory, Wright-Patterson Air Force Base, Ohio 45433, USA*

[4]*University of Dayton Research Institute, 300 College Park, Dayton, Ohio 45469, USA*

(Received 22 May 2020; revised 12 August 2020; accepted 3 September 2020; published 7 October 2020)

Functional van der Waals layered materials, which exhibit interesting phenomena such as magnetism and ferroelectricity, have been proposed for use in next-generation nanoscale devices and sensors. $CuCrP_2S_6$ is a promising two-dimensional (2D) material that evinces multiferroic behavior where the Cu^+ and Cr^{+3} cations are responsible for antiferroelectric and antiferromagnetic ordering, respectively. In this study, we use x-ray diffraction and Raman spectroscopy to map out these phase transitions in the range 70–400 K. The antiferroelectric phase transition is complex and shows a gradual transition to complete antipolar order with an intermediate quasiantipolar step. X-ray diffraction studies reveal evidence for negative thermal expansion across the antipolar phase transitions at ∼270 and ∼140 K. The latter of these is accompanied by a drastic reduction in rotational and translational mode frequencies of the anion groups in $CuCrP_2S_6$. Our temperature-dependent structural data provide an important reference for subsequent research into this promising 2D multiferroic material.

DOI: 10.1103/PhysRevMaterials.4.104003

I. INTRODUCTION

Recently, van der Waals gapped two-dimensional (2D) materials have become a main focus of research at the intersection of solid-state physics and nanomaterials. These materials, comprised of 2D sheets and their various heterostructures, are potential candidates for the next generation of electronic devices [1–3]. To this end, 2D compounds have been extensively investigated in a search for materials with conducting, insulating, semiconducting, and superconducting properties. With their tendency to form layered van der Waals gapped compounds, sulfur, selenium, and tellurium-based materials have provided for a rich vein of investigation. For example, mono- and few-layer transition metal chalcogenides, collectively referred to as TMCs, exhibit a wide range of band gaps from the infrared to ultraviolet; researchers have successfully demonstrated them for use in applications such as optoelectronics [4], logic circuits [5], energy harvesting [6], and spintronics [7], among others. However, even though some of these materials can possess strong spin-orbit coupling in the monolayer [8], they lack incipient functional properties such as magnetism and ferroelectricity which are needed for advanced device fabrication. This has led to a concerted exploration effort to discover 2D materials with functional properties for device fabrication [3,9–16]. One recent candidate, CrI_3, has been shown to exhibit ferromagnetism in the monolayer, a property which can be controlled electrically [17] or through the application of pressure [18]. However, CrI_3 and other halide-based magnets are unstable in ambient conditions due to a photocatalyzed reaction with water [19] and must necessarily be encapsulated, usually in graphene or *h*-BN. To augment the 2D materials toolbox, recent studies have advocated for fundamental structure-properties research into metal thio- and selenophospates (MTPs) [13,20,21], which exhibit properties such as ferroelectricity [22,23] and magnetism [10,24] in various compositions and have been shown to be fairly stable under ambient conditions [12,25], making them more tractable for device fabrication (e.g. [26–30]).

A particularly interesting MTP-based 2D multiferroic material is $CuCrP_2S_6$, in which antiferroelectric (AFE) and antiferromagnetic (AFM) lattices coexist on different cation sites. In Fig. 1(a) we show the 300 K structure with all atoms present. In Figs. 1(b)–1(e) we focus on the ordering of the Cu cations within their respective octahedra, with the exception of Fig. 1(e) where we also include the direction of the spin orientation on the Cr site to describe the nature of the AFM ordering. These different ferroic behaviors are associated with multiple phase transitions [31–35]: (1) There is a transition from a room-temperature paraelectric state (symmetry $C2/c$) to a quasiantipolar state at ∼190 K (T_{C1}, symmetry Pc). This phase can be described as consisting of a preferential ordering of the Cu sublattice where the Cu^{up} site has a 70% occupancy while the Cu^{down} site has a 30% occupancy [Fig. 1(a)] [34]. These occupancies alternate between the two sites in a $(\frac{1}{2}, \frac{1}{2}, 0)$ translation creating zero net electric polarization, though Ref. [34] also described it as a "glassy precursor to long-range order" which implies some degree of disorder [34]. This phase has only been structurally probed at a single temperature (160 K [34]) so we do not know if the Cu ordering is gradual, as is the case with $CuInP_2S_6$ ([22,36]) or if this is a stable configuration.

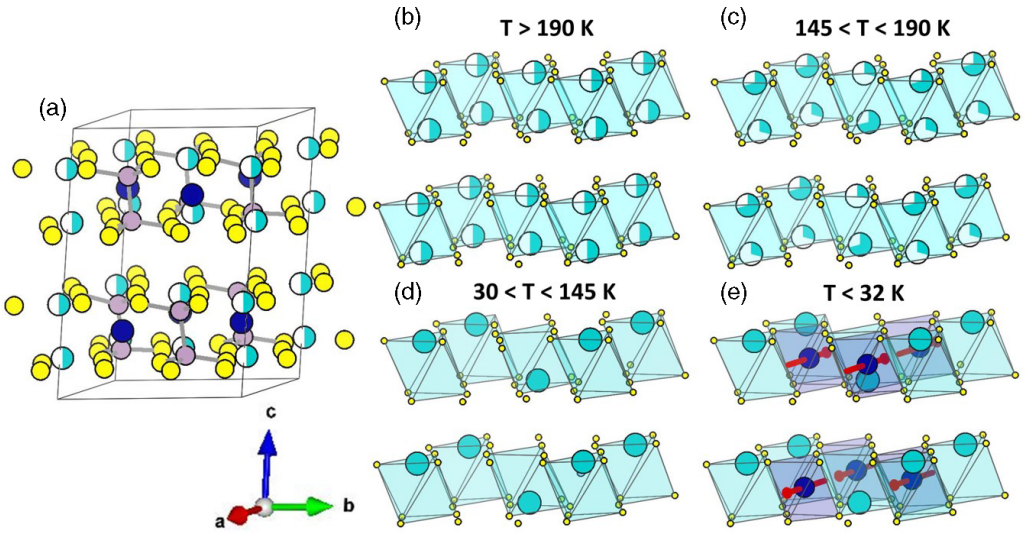

FIG. 1. Structural of $CuCrP_2S_6$ and its evolution with temperature showing differences in the crystal lattice due to the various transition temperatures associated with this system, T_{C1} (190 K), T_{C2} (145 K), and T_N (30 K). (a) Room-temperature structure showing all atoms present; yellow spheres represent S, pink spheres represent P, blue spheres represent Cr, and teal spheres represent Cu. The evolution of the phase transitions is described, for the purpose of simplicity, by focusing only on the metal cations in their respective octahedra: (b) paraelectric state where Cu is evenly divided between the up and down positions; (c) quasiantipolar state where occupancies are split 70/30 with a $(\frac{1}{2}, \frac{1}{2}, 0)$ translation (with some degree of disorder [34]) between antipolar pairs; (d) fully antipolar state with same translation as in (c); (e) multiferroic state where a magnetic moment is carried on the Cr site along the a axis. Spins are oriented along a or $-a$ in alternating layers and are denoted by the burgundy arrows. Note that the partial occupancy as presented in (c) has only been structurally probed at only one temperature (160 K [34]) so we do not know if the Cu ordering is gradual, as is the case with $CuInP_2S_6$ [22,36] or if this is a stable configuration. It is also unclear if the disorder in this phase can be described as incommensurate (cf. [32,33]).

It is also unclear if this particular phase is incommensurate as is suggested by analogy of some features in optical absorption and specific-heat studies with similar measurements performed on the ferroelectric compound $Sn_2P_2Se_6$, which also exhibits an incommensurate phase (cf. [32,33]). Thermal measurements of this transition [33] do not reveal a latent heat, thus classifying it as a second-order transition. (2) At ~145 K (T_{C2}), the occupancies become distinctly locked as Cu cations are fully confined to either a single up or down position, again in a $(\frac{1}{2}, \frac{1}{2}, 0)$ translation making this phase truly AFE, also in the Pc space group [Fig. 1(b)]. (3) There is an AFM phase at 30 K (T_N) wherein the Cr sublattice carries the magnetic moment, which lies along the ab plane [37] and has recently been theoretically modeled [25] to alternately align parallel and antiparallel to the a axis with layer [Fig. 1(d)]. From neutron-diffraction work [35], a (001) peak reflection is visible in violation of the space group Pc reflection condition $[00L]$ where $L = 2n$, indicating the presence of a sublattice described by each lamella being FM in nature with intralayer exchange interaction $J_{\text{intra}} > 0$. In turn, each FM lamella is antiferromagnetically coupled with adjacent layers ($J_{\text{inter}} < 0$) for a net zero magnetic polarization.

The ferroic properties of $CuCrP_2S_6$ have recently been theoretically investigated by Lai *et al.* [25] who noted that this material is a type-I multiferroic with (1) FM and AFE ordering likely dominant in the monolayer and (2) magnetoelectric coupling resulting from spin-orbit coupling. This opens opportunities for switchable nanoelectronics through manipulation of magnetic spins with an applied electric field. In the same report, Lai *et al.* noted the persistence of FE in poled $CuCrP_2S_6$ exfoliated sheets through piezoforce microscopy measurements. In addition, they observed spontaneous FM polarization in magnetization measurements of an inhomogeneous mixture of exfoliated nanosheets. However, they did not test for experimental confirmations of the coupling among spins, electric dipoles, and valleys or the degree of spin-orbit coupling, leading to several open questions regarding the fundamental physics of this system, both in the bulk and in the monolayer.

In order to understand the changes in the lattice brought about by the various ferroic transitions, it is important to study the temperature-dependent properties of pure single-crystalline materials. Raman spectroscopy is a particularly well-suited technique for such studies as it is quick, nondestructive, and highly expandable in terms of measuring the effects of various external variables on the vibrational modes of compounds such as pressure, temperature, and magnetic field [38]. It has been used successfully to characterize structural changes in a variety of nanomaterials such as carbon nanotubes [39], graphene [40,41], and TMDs [38], and we also expect it to help in quantifying structural changes associated with magnetic and ferroelectric transitions in $CuCrP_2S_6$ and other members of the MTP family of materials (cf. [36]), especially as these materials are developed into devices (e.g., [11,26]). Two early room-temperature Raman spectroscopy studies [42,43] revealed some general insights into the vibrational modes in $CuCrP_2S_6$, though their scopes were limited since they were written prior to the discovery of AFE ordering in $CuCrP_2S_6$ and its structural mechanism. In fact, to our knowledge, a Raman spectral study has not yet been

performed for mapping the phase transitions in $CuCrP_2S_6$ as a function of temperature. X-ray diffraction (XRD) is another characterization technique that is valuable to understand changes in the lattice structure due to atomic displacements (order-disorder or displacive transitions) during phase transitions. Detailed structural analyses derived from x-ray [22] and neutron diffraction [35,37] on $CuCrP_2S_6$ and related functional thiophosphates like $CuInP_2S_6$ have illuminated the interplay of Cu^+ movements within the unit cell and the emergence of ferroic properties. In this work, we performed temperature-dependent XRD and Raman scattering measurements on single-crystalline $CuCrP_2S_6$. Our results tie changes in the anion vibrational modes and layer spacing to changes in the Cu ordering associated with transitions to quasiantipolar (T_{C1}) and fully antipolar (T_{C2}) states. These observations can be used as a future benchmark for engineering the ferroic properties of this interesting 2D material.

II. EXPERIMENT

Synthesis and characterization. We synthesized $CuCrP_2S_6$ from pure elements (Alfa Aesar Puratronic, 99.999+%). Prior to synthesis, we reduced the Cr powder under forming gas (95% Ar, 5% H_2) to remove any oxide contamination. We weighed the elemental powder/chunks (∼3 g) to achieve a molar ratio of Cu:Cr:P:S of 1:1:2:6, with ∼5% excess P included. We ground the materials together in a mortar and pestle under an Ar environment prior to insertion into a thick-walled quartz ampoule. We then sealed the ampoule under vacuum and placed it in a tube furnace, slowly ramping the temperature to 300 °C over a period of 10 h, after which point it was held for a further 10 h. After this initial heating step, we ramped the furnace to 700 °C over a period of 13 h and held it at this setpoint for ∼7 days. We then allowed the ampoule to cool to room temperature over a period of 35 h. Upon opening the ampoule, we found crystals sized on the order of $\sim 3 \times 3\,mm^2$ which exhibited terracing common in layered materials. Physically, the crystals were flexible, grey, and micaceous. We performed elemental analysis using a Bruker Quantax 70 EDS detector coupled with a Hitachi-TM-3000 tabletop scanning electron microscope system using ten different regions. With this analysis, we determined the elemental composition of the single crystals was to be $CuCrP_2S_6$, within instrumental error. We note that the inclusion of a halide transport agent such as I_2 or a halide salt flux (e.g., $AlCl_3$/KCl) likely would engender the growth of larger crystals [44].

X-ray diffraction. We isolated flat platelets and affixed them to a mounting stub with a small quantity of Apiezon N-type vacuum grease. We performed initial measurements down to 120 K on a Rigaku SmartLab SE system with an Anton Parr DCS 500 temperature controller ($CuK_\alpha = 1.5406$ Å). To obtain a wider temperature range, we subsequently used an Oxford Chimera temperature controller mounted onto a Bruker D8 Discover DaVinci system ($CuK_\alpha = 1.5406$ Å). These results were in general agreement where they overlapped. In both experiments, we reduced the temperature to the minimum for the system (e.g.., 70 K for the Chimera) so that diffraction patterns could be taken upon heating. We collected data from $10 < 2\theta < 95^\circ$ every 5 K through 400 K. We held the temperature at the programmed temperature for 5 min prior to the start of the scan; temperature ramp rates were ∼1 K/min between scans. We fit the resulting spectra in the FULLPROF software suite [45] using Le Bail fitting of the (00l)-type peak reflections.

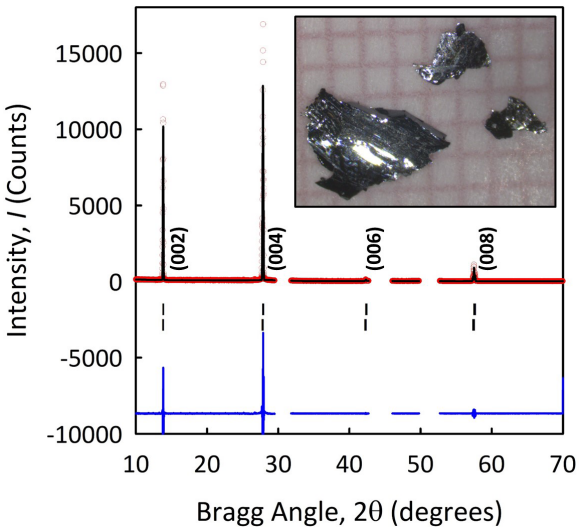

FIG. 2. XRD pattern collected at 70 K from a flat face of a single crystal showing (00l)-type peak reflections. Gaps in the pattern represent peaks resulting from the Ni-coated Cu sample holder that were excluded from the fit. The inset shows the synthesized crystals.

Raman spectroscopy. We collected temperature-dependent Raman spectra using a Renishaw inVia system. We loaded the crystals into a cold stage (Linkam Scientific, THMS600) for the low-temperature measurements. Prior to cooling, we evacuated the chamber to low pressure (∼100 mTorr), followed by backfilling with N_2. Raman spectra were collected with 633-nm excitation. The laser power was kept below 0.5 mW to avoid local laser-induced heating. Lorentzian line-shape fitting was performed on the spectra and the four most prominent peaks (room temperature peaks at ∼205, 265, 380, and 595 cm^{-1}) in the spectra were chosen for the temperature-dependent analysis.

III. RESULTS AND DISCUSSION

We isolated single crystals of $CuCrP_2S_6$ from the ampoule after synthesis conditions were completed. $CuCrP_2S_6$, like all other known MTPs, grows preferentially along the plane defined by the lamellae in this van der Waals gapped structure, which is along the *ab* plane in nearly all MTP compounds. The result is that the crystals form as flat platelets which vary from ∼100 to ∼500 μm in thickness and exhibit diameters from microscopic to ∼5 mm or larger (Fig. 2, inset). All crystallites were found to be highly terraced. These features indicate growth conditions where new nucleation sites form before growth is complete for a given layer and can potentially be controlled via careful engineering of temperature conditions, among other factors [46]. General powder diffraction on MTP materials is useful only when using higher energy synchrotron sources so we were limited to investigating the (00l)-type reflections in the material, which show excellent crystalline quality (Fig. 2).

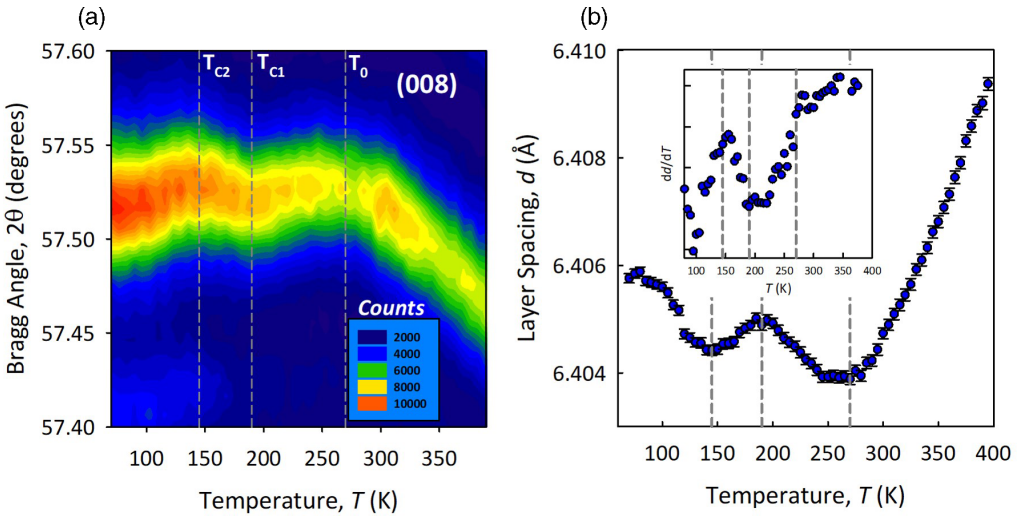

FIG. 3. (a) Heat map of the (008) reflection of the $CuCrP_2S_6$ crystal under investigation and (b) layer spacing (equal to the sum of one $CuCrP_2S_6$ lamella and one van der Waals gap) as a function of temperature. In both cases the phase transitions are denoted by the dashed grey lines.

We collected temperature-dependent XRD patterns on $CuCrP_2S_6$ single crystals between 70 and 400 K. We applied whole-pattern fitting using the Le Bail technique to the patterns collected at different temperatures. We artificially set the monoclinic angle β to 90° to plot the data in terms of layer spacing d (where d is equal to the sum of one lamella and one van der Waals gap, a common method of defining the structure in van der Waals gapped materials, cf. [16,23,36,47–49]. We present these data in Fig. 3. In Fig. 3(a), we show a heat map of the (008) peak reflection near $2\theta = 57.5°$; we focus on this peak as it is the highest-order peak reflection (and therefore least susceptible to error [50]) that displays significant intensity and is also not convoluted with peaks resulting from the experimental apparatus. The plot in Fig. 3(a) shows subtle changes in both intensity and Bragg angle with temperature, implying both (1) changes in occupancy of the Cu site as the intensity of the diffracted beam is proportional to the structure factor ($|F_{hkl}|^2$), which is in turn dependent on the occupancy of atoms in different Wyckoff positions in the unit cell, and (2) changes in the unit cell itself brought on by these changes in occupancy, which will be explored in more detail below.

In Fig. 3(b), we show the evolution of the layer spacing with temperature; the inset displays a derivative plot of the temperature data. There has been, to date, no high-temperature (i.e., between 300 K and the synthesis temperature of 973–1023 K) structural analysis of $CuCrP_2S_6$, so the possibility of phase transitions at higher temperatures, as is present in some MTP compounds (e.g., $In_{4/3}P_2S_6$ [51] and $Cu_{0.4}In_{1.2}P_2S_6$ [36]) remains an open question. However, from the literature and from the data we plot in Fig. 3, we know that $CuCrP_2S_6$ evinces a $C2/c$ structure at room temperature [37] and that there is no apparent change in structure, aside from normal thermal expansion/contraction, in the range 270–400 K. The thermal-expansion coefficient along the stacking direction calculated from these data is $\sim 10 \times 10^{-6}\,K^{-1}$, in accord with previous data collected on ferroelectric $CuInP_2S_6$ [36]. The rapid expansion of d as temperature increases likely results from the presence of enough thermal energy at these temperatures to cause the Cu to slip the confines of its potential well located near the center of the S-S-S triangle and penetrate the van der Waals gap [52] and, due to the electrostatic repulsion from these Cu cations, the expansion of the width of the gap itself.

Below 270 K, the expansion and contraction of d with temperature [Fig. 3(b)] appears to be governed by the ferroic behavior of the two cation sublattices, with higher temperature (100–270 K) behavior subject to Cu ordering and thermal displacements, and lower temperatures (<90 K) possibly dominated by Cr magnetism and frustration. At $T <$ 270 K (a point which we demarcate as T_0), d expands as temperature decreases, likely from expansion of the lamellae concomitant with the first appearance of preferential ordering of the Cu cations and/or the appearance of precursor phenomena such as antipolar clustering. We note that the location of T_0 is broadly consistent with subtle transitions noted in specific heat [33], dielectric spectroscopy [53], and ultrasonic [54] studies performed on $CuCrP_2S_6$ (where this transition appears in the 260–300 K range) and also appears to be consistent with the temperature-dependent Raman results we display below. All MTP compounds share a common $[P_2X_6]^{4-}$ structural backbone (where X = S or Se) and, as a result, have similar responses to cation ordering, so comparisons to the better-characterized ferrielectric compound $CuInP_2S_6$ are enlightening in elucidating the behavior of the structurally related $CuCrP_2S_6$ under present investigation. In $CuInP_2S_6$, the transition to the ferrielectric state is associated with a lattice *contraction* linked to 1) the reduction of the lamella thickness due to the lack of P-S deformation around the unfilled Cu site and 2) the lack of electrostatic repulsion resulting from the presence of Cu on only one side of the van der Waals gap. This behavior is in contrast to most known ferroelectrics, including $BaTiO_3$ and $PbTiO_3$, where the transition to the ferroelectric state is associated with an increase in unit-cell volume [55,56]. In contrast to the polar ordering exhibited by $CuInP_2S_6$, one

would expect that antipolar, or even quasiantipolar, ordering of the Cu cations in $CuCrP_2S_6$ would result in an *increase* in lamella thickness, which we observe [Fig. 2(b)]. This trend continues until $T = 190\,\mathrm{K}$ (T_{C1}), after which point d again decreases with temperature, likely due to the presence of an evolving incommensurate phase.

T_{C1} is the temperature associated with the second-order phase transition to a quasiantipolar state. Only one temperature in this regime has been structurally probed to date (160 K [34]), so it remains unclear whether the 70/30 copper occupancy stated in that report is constant through this phase space. Indeed, the authors of that work refer to the quasiantipolar phase as "glassy" and a precursor to long-range order which, by definition, indicates a degree of structural disorder. In addition, some authors have made a comparison between $CuCrP_2S_6$ and the well-researched ferroelectric compound $Sn_2P_2Se_6$ based on the fact that two phase transitions are present in both compounds and that they share certain features in optical absorption spectra [32] and in specific-heat analysis (cf. [33,57]). $Sn_2P_2Se_6$ forms an incommensurate phase at 220 K where a component of the wave vector of the modulated structure changes smoothly with temperature from 220 to 193 K followed by an abrupt disappearance of the satellite XRD peaks and a transition to a fully ferroelectric state at 193 K [58]. Based on these comparisons and the optical-absorption and specific-heat results, it is likely that $CuCrP_2S_6$ evinces the same property, though it has yet to be definitively proven from a structural perspective. In $Sn_2P_2Se_6$, the incommensurate phase is associated with a slight decrease in layer spacing [58], a trend we note in Fig. 2(b) for $CuCrP_2S_6$ which we ascribe to possible changes in the wave vector of the modulated structure where, increasingly, sites of high Cu cation occupancy do not directly oppose each other across the van der Waals gap, thus reducing electrostatic repulsion and layer thickness. Full structural characterization of this disordered quasiantipolar phase and its evolution with temperature are open questions which we hope to address in an upcoming publication.

The transition at 145 K is first order [33] and the structure observed in this fully antipolar state is well characterized (e.g., [37]). The Cu ordering follows a $(\frac{1}{2}, \frac{1}{2}, 0)$ translation and no Cu cations oppose each other across the van der Waals gap [Fig. 1(d)]. However, at $T < 145\,\mathrm{K}$ (T_{C2}), d again increases with decreasing T. This expansion is coincident with the rapid increase in magnetic susceptibility χ, as temperature decreases [25,59]. Curie-Weiss analysis of χ vs T plots at $100 < T < 400\,\mathrm{K}$ shows that *local* ordering of the Cr cations in $CuCrP_2S_6$ is ferromagnetic with $\theta_{CW} = 30.6\,\mathrm{K}$ [60]. These same measurements also show that *antiferromagnetic* behavior is evident at $T < 32\,\mathrm{K}$ as the lamellae couple and long-range order is achieved [60]. This competition between opposing magnetic exchange interactions has been shown to lead to negative thermal-expansion (NTE)-type behavior in other compounds, e.g., [61–63]. However, these same materials evince departures from conventional Curie-Weiss behavior which appear to be more subtle in $CuCrP_2S_6$. Previous studies [59,60] noted departures from Curie-Weiss behavior in $CuCrP_2S_6$ at $T < \sim 60\,\mathrm{K}$. Examination of the present available literature reveals some sensitivity of the determination of θ_{CW} on the data window analyzed; however, reliable data at $T > 150\,\mathrm{K}$ is currently absent from the literature, leaving this question, at the moment, unresolved for $CuCrP_2S_6$. In the Cr-containing chalcogenide $LiGaCr_4S_8$, competing AFM and FM exchange interactions are present which, when combined with strong coupling between the lattice and the magnetic ground state, result in negative thermal expansion (NTE) from 110 to ∼10 K [62]. If similar dynamics are present in $CuCrP_2S_6$ where similarly strong lattice couplings are predicted from theory [25], it is likely that the layer thickness will again decrease as long-range AFM order is established at 32 K, as in the observations of $LiGaCr_4S_8$ [62]. Future investigation regarding detailed structural analysis of the NTE phenomenon, magnetic behavior, and the interplay of cation ordering and local deformations in the $CuCrP_2S_6$ lamellae will likely be fruitful, especially given our current limitations both in availability of temperatures probed and in structural parameters analyzed. Nevertheless, magnetic 2D NTE materials are not only interesting from a fundamental perspective due to the complex physics involved, but are also interesting from an applications perspective since NTE materials, when mated with other 2D materials, help form zero thermal-expansion devices necessary for complex optics [64].

Next, we turn to temperature-dependent Raman spectroscopy measurements to probe the $CuCrP_2S_6$ vibrational modes across the phase transitions. We collected polarized Raman spectra in the backscattering geometry (with the incident laser perpendicular to the crystal surface) as a function of temperature from 77 to 350 K. We used a polarization rotator to set the laser polarization to vertical (VH) or horizontal (HH); we kept the scattered light horizontally polarized. Figure 4 shows example spectra collected at room temperature (297 K) and at 100 K. A number of modes can be observed in the low-temperature spectra, some of which are distinct between the VH and HH polarizations. At the same time, there are several peaks that appear in both spectra, suggesting depolarization effects which can be attributed to steps and dislocations on the crystal surfaces. An additional source of the extra peaks in the low-temperature spectra could be the appearance of infrared-active phonon modes due to the lowering of crystal inversion symmetry [43] associated with the ferroic phase transitions. In the room-temperature spectrum, however, almost all of the peaks observed in our measured spectral range (50–700 cm^{-1}) can be assigned to anion vibrations. The modes corresponding to the metal cation vibrations fell below our measured spectral range.

For the temperature-dependent peak frequency and width analysis, we chose four peaks labeled *a*-*d* in Fig. 4. Of these four peaks, only peak *a* corresponds to a vibrational mode of the E_g type; its intensity does not diminish in the VH spectrum. All other peaks correspond to A_g modes and their intensities are drastically reduced in the VH spectrum. A comparison of our measured Raman peaks with those published in the literature reveals that the peaks *a, b, c*, and *d* correspond to rotations (R'), translations (T'), and symmetric stretching and deformation of PS_3 groups (ν_1 and ν_2) within the $[P_2S_6]^{4-}$ ethanelike building blocks of the anion sublattice, respectively [42,65]. These vibrational modes are associated with the anion sublattice responding to movements of the Cu cations within the S_6 octahedra with the onset of antiferroelectric ordering. To see the effect of the phase transitions on the phonon modes, we analyzed the peak frequencies and linewidths (full width

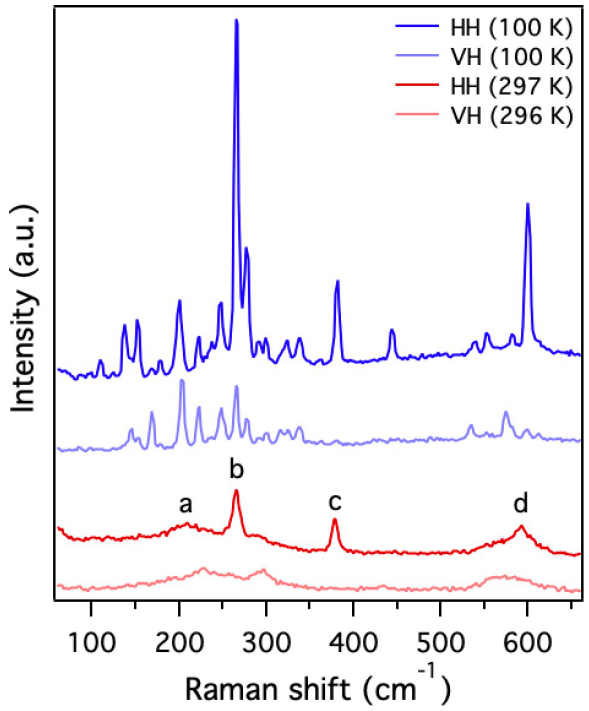

FIG. 4. Plane- (HH) and cross-polarized (VH) Raman spectra collected in the backscattered geometry from $CuCrP_2S_6$ single crystals. The four prominent peaks in the room temperature spectrum, labeled *a*, *b*, *c*, and *d* were used for analysis of temperature-dependent peak frequencies and linewidths.

at half maximum intensity) of these four peaks over our measured temperature range. Owing to their higher signal to noise, we chose only the HH polarized spectra for the analysis.

As mentioned above and demonstrated in previous studies [34,35], the antipolar and quasiantipolar phase transitions in $CuCrP_2S_6$ take place by the hopping and ordering of Cu ions within the lamellae. This atomic rearrangement is expected to affect the phonon mode frequencies and can be observed in the temperature-dependent Raman spectra. While we could not directly measure the phonon modes of the cations owing to their frequencies being outside of our measurement range, it is still instructive to see the effect of the phase transitions on the anion phonon modes. The temperature-dependent Raman frequencies and widths of the four modes from Fig. 4 are plotted in Fig. 5. The phase-transition temperatures are shown for reference as dashed vertical lines.

All four peaks exhibit interesting temperature dependencies. The two low-frequency anion rotation [Fig. 5(a), (R')] and translation modes [Fig. 5(c), (T')] increase in frequency (i.e., harden) as the temperature is reduced from 350 K. This is the expected behavior for all anharmonic solids where peak frequency increases (decreases) with decreasing (increasing) temperature [66]. We note that T_0 coincides with a subtle shift in the slope of the frequency shift vs temperature for the rotational and translational modes, indicating that the transition to the quasiantipolar state is likely gradual. However, around 190 K (T_{C1}), the slope in frequency abruptly changes, indicating the boundary between the paraelectric and quasiantipolar states. This is concomitant with the region of layer expansion seen in Fig. 3(b) in the XRD data. Interestingly, the frequency of the PS_3 rotational mode decreases slightly between T_{C1} and T_{C2} [Fig. 5(a)] while the translational mode frequency remains almost constant [Fig. 5(c)]. This latter effect, an invariance in peak frequency, indicates a stabilization brought about in the lattice by the reduction in the thermal hopping of Cu ions during the transition to the quasiantipolar state.

Once the crystal goes into the fully antipolar AFE phase below 145 K ($T < T_{C2}$), the rotational and translational mode frequencies soften, in conjunction with the increase in layer thickness (and NTE) observed in the XRD data (Fig. 3). This kind of behavior is usually expected with soft modes [67,68] wherein an unstable phonon mode condenses (i.e., its frequency goes down to zero) across a phase transition. Here we do not observe the complete condensation of the two modes in the AFE phase; in fact, we observe a slight increase in frequency around our lowest measured temperature (77 K). Since the AFE transition occurs by the complete ordering of the Cu ions in the up or down states, one might expect soft-mode behavior in the cation vibrational modes. However, this has not been observed in the literature for other layered thiophosphates like $CuInP_2S_6$ [69]. Moreover, we also do not expect soft-mode behavior in the anion (PS_3) vibrational modes. However, our observations [as shown in Figs. 4(a) and 4(b)] highlight the cooperation between the cation and anion vibrations, and we attribute the softening of the PS_3 rotational and translational modes in the AFE phase to the influence of the reordering of the Cu cations below T_{C2}. This kind of coupling between Cu ions and PS_3 vibrational modes has been previously observed in $CuInP_2S_6$ [22]. The coupling-induced softening of the PS_3 (effectively the P_2S_6 octahedra) modes could also play a role in the decrease in lattice spacing as observed in our XRD study [Fig. 3(b)]. Indeed, soft-mode-like behavior of the rotational and translational modes in complex oxides has been related to NTE in those materials [70]. The two stretching modes [*c* and *d* in Fig. 4, denoted by the symbols ν_1 and ν_2 in Fig. 5] exhibit hardening as the temperature is reduced from 350 K to T_{C1} [Figs. 5(e) and 5(g)]. In the quasiantipolar phase ($T_{C2} < T < T_{C1}$), the peak frequencies do not become constant as they did for the rotational and stretching modes. Below T_{C2}, in the AFE phase one stretching mode continues to harden [ν_1, Fig. 5(e)] while the other mode frequency [ν_2, Fig. 5(g)] exhibits a slight decrease with decreasing temperature until ~100 K. Our observed trends in the temperature-dependent peak frequencies show that the rotational and translational phonon modes play a larger role than the stretching modes in the structural instabilities across both phase-transition temperatures.

The peak widths of the rotational and translational modes also follow the expected trends in the high-temperature regime ($T > T_{C1}$), where they decrease (peak sharpening) with decreasing temperature from 350 K to T_{C1} [Figs. 5(b), 5(d), 5(f), and 5(h)]. Sharpening of Raman peaks with decreasing temperatures is expected for anharmonic phonon modes wherein the decay channels decrease (typically optical phonons decay into lower energy acoustic phonons), resulting in longer lifetimes and hence sharper peaks [66]. However, in the quasiantipolar phase ($T_{C2} < T < T_{C1}$), the peak widths remain almost constant or slightly decrease, reflecting the trends observed in the peak frequencies. Below T_{C2} in the AFE phase,

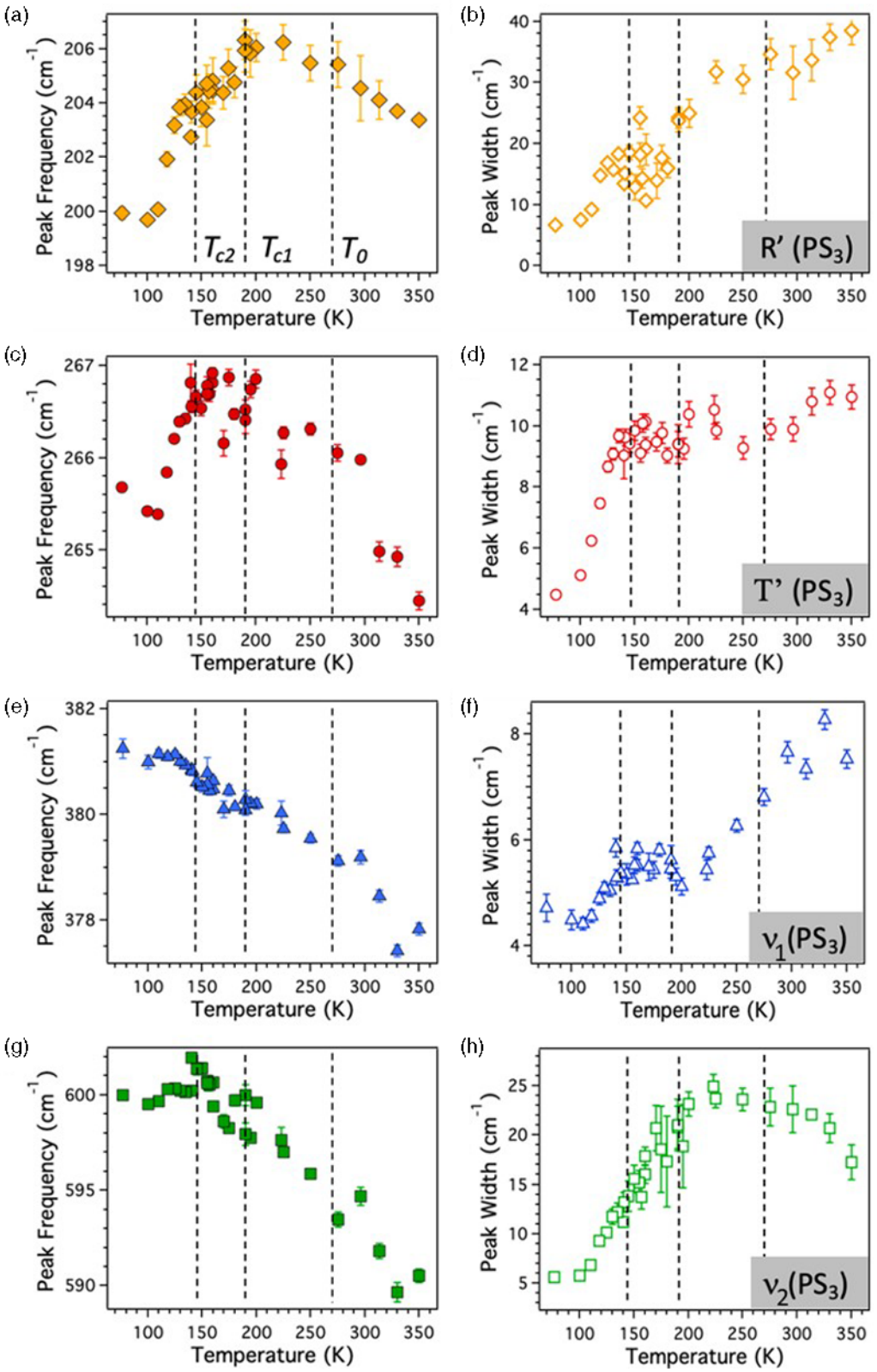

FIG. 5. Temperature-dependent peak frequencies [(a), (c), (e), and (g)] and peak widths [(b), (d), (f), and (h)], respectively, of four vibrational modes in $CuCuP_2S_6$. The phase-transition temperatures are shown by the vertical dashed lines. The rotational, translational, and stretching modes are denoted by R', T', and ν_1 and ν_2, respectively. The error bars correspond to the standard deviation error resulting from the peak fitting procedure.

they decrease sharply down to about 100 K beyond which they again begin to increase. All four peak widths behave in a similar fashion with varying degrees of change.

IV. CONCLUSION

In this work, we have shown that the van der Waals gapped 2D multiferroic compound $CuCrP_2S_6$ contains multiple structural phase transitions that are accessible to both XRD and Raman analysis. These transitions are associated with structural changes which accompany AFE and AFM ordering on the Cu and Cr cation sublattices, respectively. In the former case, AFE ordering manifests as a gradual transition to a quasiantipolar state at around 190 K followed by a further transition to a fully antipolar state at 145 K. These complex transitions are associated with subtle changes in layer thickness as measured through x-ray diffraction and traceable differences in Raman peak frequencies and widths. In addition, from the diffraction data we see possible negative thermal expansion at low temperatures which may be attributed to the presence of competing ferromagnetic and antiferromagnetic ground states. The exact nature of the coupling between the magnetic and ferroelectric properties and the lattice itself remains an open question and will be the subject of intense future investigation. Our temperature-dependent structural data provide an important reference for subsequent research into this interesting 2D multiferroic material.

ACKNOWLEDGMENTS

The authors are grateful for funding support from AFOSR (Grants No. LRIR 16RXCOR322, No. LRIR 19RXCOR052, and No. LRIR 18RQCOR100) and AFRL/RX (Lab Director's Funds). The authors also wish to acknowledge the contributions of J. Cory, who developed the Python code to automate the Chimera low-temperature attachment. We would also like to thank Prof. B. Lv at the University of Texas at Dallas for enlightening discussions. Finally, the authors are grateful to L. M. Zevorich Susner for her help in manuscript editing and preparation.

[1] A. K. Geim and I. V. Grigorieva, Van der Waals heterostructures, Nature (London) **499**, 419 (2013).

[2] L. D. Casto, A. J. Clune, M. O. Yokosuk, J. L. Musfeldt, T. J. Williams, H. L. Zhuang, M.-W. Lin, K. Xiao, R. G. Hennig, B. C. Sales, J.-Q. Yan, and D. Mandrus, Strong spin-lattice coupling in $CrSiTe_3$, APL Mater. **3**, 041515 (2015).

[3] C. Gong and X. Zhang, Two-dimensional magnetic crystals and emergent heterostructure devices, Science **363**, eaav4450 (2019).

[4] B. W. H. Baugher, H. O. H. Churchill, Y. Yang, and P. Jarillo-Herrero, Optoelectronic devices based on electrically tunable p-n diodes in a monolayer dichalcogenide, Nat. Nanotechnol. **9**, 262 (2014).

[5] J.-K. Huang, J. Pu, C.-L. Hsu, M.-H. Chiu, Z.-Y. Juang, Y.-H. Chang, W.-H. Chang, Y. Iwasa, T. Takenobu, and L.-J. Li, Large-area synthesis of highly crystalline WSe_2 monolayers and device applications, ACS Nano **8**, 923 (2014).

[6] F. R. Fan and W. Wu, Emerging devices based on two-dimensional monolayer materials for energy harvesting, Research **2019**, 7367828 (2019).

[7] H. Li, S. Ruan, and Y. Zeng, Intrinsic van der waals magnetic materials from bulk to the 2D limit: new frontiers of spintronics, Adv. Mater. **31**, 1900065 (2019).

[8] N. Zibouche, A. Kuc, J. Musfeldt, and T. Heine, Transition-metal dichalcogenides for spintronic applications: Spintronics beyond graphene, Ann. Phys. **526**, 395 (2014).

[9] L. Niu, F. Liu, Q. Zeng, X. Zhu, Y. Wang, P. Yu, J. Shi, J. Lin, J. Zhou, Q. Fu, W. Zhou, T. Yu, X. Liu, and Z. Liu, Controlled synthesis and room-temperature pyroelectricity of $CuInP_2S_6$ ultrathin flakes, Nano Energy **58**, 596 (2019).

[10] X. Wang, K. Du, Y. Y. Fredrik Liu, P. Hu, J. Zhang, Q. Zhang, M. H. S. Owen, X. Lu, C. K. Gan, P. Sengupta, C. Kloc, and Q. Xiong, Raman spectroscopy of atomically thin two-dimensional magnetic iron phosphorus trisulfide ($FePS_3$) crystals, 2D Mater. **3**, 031009 (2016).

[11] J. Chu, F. Wang, L. Yin, L. Lei, C. Yan, F. Wang, Y. Wen, Z. Wang, C. Jiang, L. Feng, J. Xiong, Y. Li, and J. He, High-performance ultraviolet photodetector based on a few-layered 2D $NiPS_3$ nanosheet, Adv. Funct. Mater. **27**, 1701342 (2017).

[12] J. A. Brehm, S. M. Neumayer, L. Tao, A. O'Hara, M. Chyasnavichus, M. A. Susner, M. A. McGuire, S. V. Kalinin, S. Jesse, P. Ganesh, S. T. Pantelides, P. Maksymovych, and N. Balke, Tunable quadruple-well ferroelectric van der Waals crystals, Nat. Mater. **19**, 43 (2020).

[13] F. Wang, Z. Wang, L. Yin, R. Cheng, J. Wang, Y. Wen, T. A. Shifa, F. Wang, Y. Zhang, X. Zhan, and J. He, 2D library beyond graphene and transition metal dichalcogenides: a focus on photodetection, Chem. Soc. Rev. **47**, 6296 (2018).

[14] R. Kumar, R. N. Jenjeti, and S. Sampath, Two-dimensional, few-layer $MnPS_3$ for selective NO_2 gas sensing under Ambient Conditions, ACS Sens. **5**, 404 (2020).

[15] X. Wang, J. Wang, J. Wang, B. Wei, and Z. Wang, Atomic structure and electronic property of two-dimensional ferroelectric $CuInP_2Se_6$, Ceram. Int. **46**, 7014 (2020).

[16] M. A. McGuire, J. Yan, P. Lampen-Kelley, A. F. May, V. R. Cooper, L. Lindsay, A. Puretzky, L. Liang, S. KC, E. Cakmak, S. Calder, and B. C. Sales, High-temperature magnetostructural transition in van der Waals-layered α-$MoCl_3$, Phys. Rev. Mater. **1**, 064001 (2017).

[17] B. Huang, G. Clark, D. R. Klein, D. MacNeill, E. Navarro-Moratalla, K. L. Seyler, N. Wilson, M. A. McGuire, D. H. Cobden, D. Xiao, W. Yao, P. Jarillo-Herrero, and X. Xu, Electrical control of 2D magnetism in bilayer CrI_3, Nat. Nanotechnol. **13**, 544 (2018).

[18] T. Li, S. Jiang, N. Sivadas, Z. Wang, Y. Xu, D. Weber, J. E. Goldberger, K. Watanabe, T. Taniguchi, C. J. Fennie, K. Fai Mak, and J. Shan, Pressure-controlled interlayer magnetism in atomically thin CrI_3, Nat. Mater. **18**, 1303 (2019).

[19] D. Shcherbakov, P. Stepanov, D. Weber, Y. Wang, J. Hu,

Y. Zhu, K. Watanabe, T. Taniguchi, Z. Mao, W. Windl, J. Goldberger, M. Bockrath, and C. N. Lau, Raman spectroscopy, photocatalytic degradation, and stabilization of atomically thin chromium tri-iodide, Nano Lett. **18**, 4214 (2018).

[20] M. A. Susner, M. Chyasnavichyus, M. A. McGuire, P. Ganesh, and P. Maksymovych, Metal thio- and selenophosphates as multifunctional van der waals layered materials, Adv. Mater. **29**, 1602852 (2017).

[21] W. Huang, F. Wang, L. Yin, R. Cheng, Z. Wang, M. G. Sendeku, J. Wang, N. Li, Y. Yao, and J. He, Gate-coupling-enabled robust hysteresis for nonvolatile memory and programmable rectifier in van der waals ferroelectric heterojunctions, Adv. Mater. **32**, 1908040 (2020).

[22] V. Maisonneuve, V. B. Cajipe, A. Simon, R. Von Der Muhll, and J. Ravez, Ferrielectric ordering in lamellar $CuInP_2S_6$, Phys. Rev. B **56**, 10860 (1997).

[23] M. A. Susner, A. Belianinov, A. Y. Borisevich, Q. He, M. Chyasnavichyus, P. Ganesh, H. Demir, D. Sholl, D. L. Abernathy, M. A. McGuire, and P. Maksymovych, High T_c layered ferrielectric crystals by coherent spinodal decomposition, ACS Nano **9**, 12365 (2015).

[24] A. R. Wildes, V. Simonet, E. Ressouche, G. J. McIntyre, M. Avdeev, E. Suard, S. A. J. Kimber, D. Lançon, G. Pepe, B. Moubaraki, and T. J. Hicks, Magnetic structure of the quasi-two-dimensional antiferromagnet $NiPS_3$, Phys. Rev. B **92**, 224408 (2015).

[25] Y. Lai, Z. Song, Y. Wan, M. Xue, C. Wang, Y. Ye, L. Dai, Z. Zhang, W. Yang, H. Du, and J. Yang, Two-dimensional ferromagnetism and driven ferroelectricity in van der Waals $CuCrP_2S_6$, Nanoscale **11**, 5163 (2019).

[26] M. Si, A. K. Saha, P.-Y. Liao, S. Gao, S. M. Neumayer, J. Jian, J. Qin, N. Balke Wisinger, H. Wang, P. Maksymovych, W. Wu, S. K. Gupta, and P. D. Ye, Room-temperature electrocaloric effect in layered ferroelectric $CuInP_2S_6$ for solid-state refrigeration, ACS Nano **13**, 8760 (2019).

[27] Y. Gao, S. Lei, T. Kang, L. Fei, C.-L. Mak, J. Yuan, M. Zhang, S. Li, Q. Bao, Z. Zeng, Z. Wang, H. Gu, and K. Zhang, Bias-switchable negative and positive photoconductivity in 2D $FePS_3$ ultraviolet photodetectors, Nanotechnology **29**, 244001 (2018).

[28] R. Kumar, R. N. Jenjeti, M. P. Austeria, and S. Sampath, Bulk and few-layer $MnPS_3$: a new candidate for field effect transistors and UV photodetectors, J. Mater. Chem. C **7**, 324 (2019).

[29] J. Liu, Y. Wang, Y. Fang, Y. Ge, X. Li, D. Fan, and H. Zhang, A robust 2D photo-electrochemical detector based on $NiPS_3$ flakes, Adv. Electron. Mater. **5**, 1900726 (2019).

[30] J. Wu, H.-Y. Chen, N. Yang, J. Cao, X. Yan, F. Liu, Q. Sun, X. Ling, J. Guo, and H. Wang, High tunnelling electroresistance in a ferroelectric van der Waals heterojunction via giant barrier height modulation, Nat. Electron. **3**, 466 (2020).

[31] A. Dziaugys, V. V. Shvartsman, J. Macutkevic, J. Banys, Y. Vysochanskii, and W. Kleemann, Phase diagram of mixed $Cu(In_xCr_{1-x})P_2S_6$ crystals, Phys. Rev. B **85**, 134105 (2012).

[32] I. P. Studenyak, O. A. Mykajlo, Y. M. Vysochanskii, and V. B. Cajipe, Optical absorption studies of phase transitions in $CuCrP_2S_6$ layered antiferroelectrics, J. Phys.: Condens. Matter **15**, 6773 (2003).

[33] K. Moriya, N. Kariya, A. Inaba, T. Matsuo, I. Pritz, and Y. M. Vysochanskii, Low-temperature calorimetric study of phase transitions in $CuCrP_2S_6$, Solid State Commun. **136**, 173 (2005).

[34] V. B. Cajipe, J. Ravez, V. Maisonneuve, A. Simon, C. Payen, R. Von Der Muhll, and J. E. Fischer, Copper ordering in lamellar $CuMP_2S_6$(M = Cr, In) : Transition to an antiferroelectric or ferroelectric phase, Ferroelectrics **185**, 135 (1996).

[35] V. Maisonneuve, C. Payen, and V. B. Cajipe, On CuCrPS: copper disorder, stacking distortions, and magnetic ordering, J. Solid State Chem. **116**, 208 (1995).

[36] M. A. Susner, M. Chyasnavichyus, A. A. Puretzky, Q. He, B. S. Conner, Y. Ren, D. A. Cullen, P. Ganesh, D. Shin, H. Demir, J. W. McMurray, A. Y. Borisevich, P. Maksymovych, and M. A. McGuire, Cation-eutectic transition *via* sublattice melting in $CuInP_2S_6/In_{4/3}P_2S_6$ van der waals layered crystals, ACS Nano **11**, 7060 (2017).

[37] V. Maisonneuve, V. B. Cajipe, and C. Payen, Low-temperature neutron powder diffraction study of copper chromium thiophosphate ($CuCrP_2S_6$): observation of an ordered, antipolar copper sublattice, Chem. Mater. **5**, 758 (1993).

[38] R. Saito, Y. Tatsumi, S. Huang, X. Ling, and M. S. Dresselhaus, Raman spectroscopy of transition metal dichalcogenides, J. Phys.: Condens. Matter **28**, 353002 (2016).

[39] R. Rao, A. E. Islam, J. Carpena-Nunez, P. Nikolaev, B. Maruyama, R. Rao, A. E. Islam, J. Carpena-Nunez, P. Nikolaev, C. L. Pint, R. S. Weatherup, R. S. Weatherup, S. Hofmann, E. R. Meshot, F. Fornasiero, F. Wu, C. Zhou, N. Dee, A. J. Hart, P. B. Amama *et al.*, Carbon nanotubes and related nanomaterials: critical advances and challenges for synthesis toward mainstream commercial applications, ACS Nano **12**, 11756 (2018).

[40] M. Paillet, R. Parret, J.-L. Sauvajol, and P. Colomban, Graphene and related 2D materials: An overview of the raman studies: graphene and related 2D materials, J. Raman Spectrosc. **49**, 8 (2018).

[41] A. E. Islam, S. S. Kim, R. Rao, Y. Ngo, J. Jiang, P. Nikolaev, R. Naik, R. Pachter, J. Boeckl, and B. Maruyama, Photothermal oxidation of single layer graphene, RSC Adv. **6**, 42545 (2016).

[42] O. Poizat and C. Sourisseau, A comparative vibrational study of $Cr^{III}{}_{05}M^{I}{}_{05}PS_3$ and $Mn^{II}{}_{1-x}M^{I}{}_{2x}PS_3$ layer-type compounds with M^I = Cu(x = 013) and Ag (x = 05), J. Solid State Chem. **59**, 371 (1985).

[43] C. Payen, P. McMillan, and P. Colombet, A Raman spectroscopic study of some $MM'P_2S_6$ layered phases [M = Cu , Ag, Cd; M′ = Sc , V, Cr, Fe, In], Eur. J. Solid State Inorg. Chem. **27**, 881 (1990).

[44] J.-Q. Yan, B. C. Sales, M. A. Susner, and M. A. McGuire, Flux growth in a horizontal configuration: An analog to vapor transport growth, Phys. Rev. Mater. **1**, 023402 (2017).

[45] C. Frontera and J. Rodriguez-Carvajal, FULLPROF as a new tool for flipping ratio analysis: further improvements, Phys. B (Amsterdam, Neth.) **350**, e731 (2004).

[46] H. Weishart and E. Bauser, Growth conditions for improving the quality of semiconductor single crystal materials, Mater. Sci. Eng., A **173**, 33 (1993).

[47] M. A. McGuire, H. Dixit, V. R. Cooper, and B. C. Sales, Coupling of crystal structure and magnetism in the layered, ferromagnetic insulator CrI_3, Chem. Mater. **27**, 612 (2015).

[48] M. A. McGuire, G. Clark, S. Kc, W. M. Chance, G. E. Jellison, V. R. Cooper, X. Xu, and B. C. Sales, Magnetic behavior and spin-lattice coupling in cleavable van der Waals layered $CrCl_3$ crystals, Phys. Rev. Mater. **1**, 014001 (2017).

[49] M. McGuire, Crystal and magnetic structures in layered,

transition metal dihalides and trihalides, Crystals **7**, 121 (2017).

[50] B. D. Cullity, *Elements of X-Ray Diffraction*, 1st ed. (Addison-Wesley, Reading, MA, 1956), p. 332.

[51] V. Y. Gebesh, M. V. Potorii, and Y. V. Voroshilov, Phase equilibrium in the In-P-S system, Ukr. Khim. Zhurn. **57**, 803 (1991).

[52] N. Balke, S. M. Neumayer, J. A. Brehm, M. A. Susner, B. J. Rodriguez, S. Jesse, S. V. Kalinin, S. T. Pantelides, M. A. McGuire, and P. Maksymovych, Locally controlled Cu-Ion transport in layered ferroelectric $CuInP_2S_6$, ACS Appl. Mater. Interfaces **10**, 27188 (2018).

[53] A. Dziaugys, Influence of Impurities on Dielectric Properties of Ferroelectric and Superionic Crystals, Ph.D. dissertation, Vilnius University, 2011.

[54] V. Samulionis, Acoustic and piezoelectric properties of new polar semiconductor compounds of $Sn_2P_2S_6$ family, Ultragarsas **4**, 7 (2002).

[55] T. Nakatani, A. Yoshiasa, A. Nakatsuka, T. Hiratoko, T. Mashimo, M. Okube, and S. Sasaki, Variable-temperature single-crystal X-ray diffraction study of tetragonal and cubic perovskite-type barium titanate phases, Acta Crystallogr. Sect. B: Struct. Sci., Cryst. Eng. Mater. **72**, 151 (2016).

[56] A. Yoshiasa, T. Nakatani, A. Nakatsuka, M. Okube, K. Sugiyama, and T. Mashimo, High-temperature single-crystal X-ray diffraction study of tetragonal and cubic perovskite-type $PbTiO_3$ phases, Acta Crystallogr. Sect. B: Struct. Sci., Cryst. Eng. Mater. **72**, 381 (2016).

[57] K. Moriya, T. Yamada, K. Sakai, S. Yano, S. Baluja, T. Matsuo, I. Pritz, and Y. M. Vysochanskii, Ferroelectric phase transitions in $Pb_{2x}Sn_{2(1-x)}P_2Se_6$ system, J. Therm. Anal. Calorim. **70**, 321 (2002).

[58] T. K. Barsamian, S. S. Khasanov, V. S. Shekhtman, Y. M. Vysochanskii, and V. Y. Slivka, Incommensurate phase in proper ferroelectric $Sn_2P_2Se_6$, Ferroelectrics **67**, 47 (1986).

[59] P. Colombet, A. Leblanc, M. Danot, and J. Rouxel, Structural aspects and magnetic properties of the lamellar compound copper chromium phosphorotrithioite $Cu_{050}Cr_{050}PS_3$), J. Solid State Chem. **41**, 174 (1982).

[60] W. Kleemann, V. V. Shvartsman, P. Borisov, J. Banys, and Y. M. Vysochanskii, Magnetic and polar phases and dynamical clustering in multiferroic layered solid solutions $CuCr_{1-x}In_xP_2S_6$, Phys. Rev. B **84**, 094411 (2011).

[61] X. L. Chen, Z. R. Yang, W. Tong, Z. H. Huang, L. Zhang, S. L. Zhang, W. H. Song, L. Pi, Y. P. Sun, M. L. Tian, and Y. H. Zhang, Study of negative thermal expansion in the frustrated spinel $ZnCr_2Se_4$, J. Appl. Phys. **115**, 083916 (2014).

[62] G. Pokharel, A. F. May, D. S. Parker, S. Calder, G. Ehlers, A. Huq, S. A. J. Kimber, H. S. Arachchige, L. Poudel, M. A. McGuire, D. Mandrus, and A. D. Christianson, Negative thermal expansion and magnetoelastic coupling in the breathing pyrochlore lattice material $LiGaCr_4S_8$, Phys. Rev. B **97**, 134117 (2018).

[63] J. Hemberger, H.-A. K. von Nidda, V. Tsurkan, and A. Loidl, Large Magnetostriction and Negative Thermal Expansion in the Frustrated Antiferromagnet $ZnCr_2Se_4$, Phys. Rev. Lett. **98**, 147203 (2007).

[64] J. P. Attfield, Mechanisms and materials for NTE, Front. Chem. **6**, 371 (2018).

[65] C. Sourisseau, J. P. Forgerit, and Y. Mathey, Vibrational study of the $[P_2S_6{}^4-]$ anion, of some MPS_3 layered compounds (M = Fe , Co, Ni, $In_{2/3}$, and of their intercalates with $[Co(\eta^5 - C_5H_5)_2{}^+]$ cations, J. Solid State Chem. **49**, 134 (1983).

[66] G. Lucazeau, Effect of pressure and temperature on Raman spectra of solids: anharmonicity, J. Raman Spectrosc. **34**, 478 (2003).

[67] G. Venkataraman, Soft modes and structural phase transitions, Bull. Mater. Sci. **1**, 129 (1979).

[68] T. Shigenari, Raman spectra of soft modes in ferroelectric crystals, *Ferroelectric Materials - Synthesis and Characterization* (IntechOpen, 2015).

[69] Y. M. Vysochanskii, V. A. Stephanovich, A. A. Molnar, V. B. Cajipe, and X. Bourdon, Raman spectroscopy study of the ferrielectric-paraelectric transition in layered $CuInP_2S_6$, Phys. Rev. B **58**, 9119 (1998).

[70] R. Mittal, M. K. Gupta, and S. L. Chaplot, Phonons and anomalous thermal expansion behaviour in crystalline solids, Prog. Mater. Sci. **92**, 360 (2018).